

**A Measurement of the Left-Right Cross Section Asymmetry in Z^0 Production
with Polarized e^+e^- Collisions***

Hwanbae Park

Stanford Linear Accelerator Center
Stanford University
Stanford, CA 94309

SLAC-Report-691
December 1993

Prepared for the Department of Energy
under contract number DE-AC03-76SF00515

Printed in the United States of America. Available from the National Technical Information Service, U.S. Department of Commerce, 5285 Port Royal Road, Springfield, VA 22161.

* Ph.D. thesis, University of Oregon, Eugene, OR 97403

A MEASUREMENT OF THE LEFT-RIGHT CROSS SECTION
ASYMMETRY IN Z^0 PRODUCTION WITH
POLARIZED e^+e^- COLLISIONS

by

HWANBAE PARK

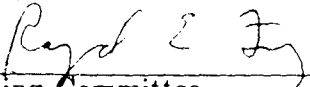
A DISSERTATION

Presented to the Department of Physics
and the Graduate School of the University of Oregon
in partial fulfillment of the requirements

for the degree of
Doctor of Philosophy

December 1993

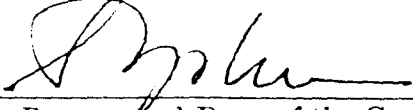
"A Measurement of the Left-Right Cross Section Asymmetry in Z^0 Production with Polarized e^+e^- Collisions," a dissertation prepared by Hwanbae Park in partial fulfillment of the requirements for the Doctor of Philosophy degree in the Department of Physics. This dissertation has been approved and accepted by:


Chair of the Examining Committee

December 15, 1993
Date

Committee in charge: Dr. Raymond E. Frey, Chair
 Dr. James E. Brau
 Dr. Nilendra G. Deshpande
 Dr. James N. Imamura
 Dr. Robert M. Mazo

Accepted by:


Vice Provost and Dean of the Graduate School

An Abstract of the Dissertation of

Hwanbae Park for the degree of Doctor of Philosophy
in the Department of Physics to be taken December 1993

Title: A MEASUREMENT OF THE LEFT-RIGHT CROSS SECTION
ASYMMETRY IN Z^0 PRODUCTION WITH
POLARIZED e^+e^- COLLISIONS

Approved: _____

Dr. Raymond E. Frey

The Stanford Linear Collider at SLAC is an e^+e^- collider running at $\sqrt{s} \approx M_Z$ and has provided an electron beam with longitudinal polarization at the SLC interaction point. The 1992 polarized run data were taken with the SLD detector. We present here the measurement of the left-right cross section asymmetry (A_{LR}) for the 1992 run.

The polarized run began in May and ended in September of 1992 at a mean center-of-mass energy of 91.56 GeV. Tower hit information of the liquid argon calorimeter and endcap warm iron calorimeter pads were used for selecting hadronic Z^0 or tau pair events. The SLD detector collected about 11,000 events during this run.

The magnitude of the longitudinal polarization of the electron beam was continuously measured by a polarimeter based on Compton scattering, and was monitored by a polarimeter based on Moller scattering. The luminosity-weighted average longitudinal polarization during the 1992 run was measured as 22.4 ± 0.6 (syst.)%.

From these data, the value of A_{LR} has been measured to be $0.102 \pm$

0.044 (stat.) ± 0.003 (syst.), corresponding to an effective electroweak mixing angle ($\sin^2 \theta_w^{\text{eff}}$) of 0.2375 ± 0.0056 (stat.) ± 0.0004 (syst.). The error is dominated by the statistical error. This value of $\sin^2 \theta_w^{\text{eff}}$ is in good agreement with existing measurements from other experiments. Studies of improvements in A_{LR} event selection for future high-statistics runs are also discussed.

CURRICULUM VITA

NAME OF AUTHOR: Hwanbae Park

PLACE OF BIRTH: Kyungsangbuk-Do, Republic of Korea

DATE OF BIRTH: December 15, 1960

GRADUATE AND UNDERGRADUATE SCHOOLS ATTENDED:

University of Oregon
Sogang University

DEGREES AWARDED:

Doctor of Philosophy, 1993, University of Oregon
Master of Science, 1989, University of Oregon
Bachelor of Arts, 1983, Sogang University

AREAS OF SPECIAL INTEREST:

Experimental High Energy Physics

PROFESSIONAL EXPERIENCE:

Research Assistant, Department of Physics, University of Oregon,
Eugene, 1990-1993

Research Assistant, Department of Physics, Sogang University,
Seoul, 1983-1985

Teaching Assistant, Department of Physics, Sogang University,
Seoul, 1983-1984

PUBLICATIONS:

- [1] K. Abe, *et. al.*, Phys. Rev. Lett. **71** (1993) 2528.
- [2] K. Abe, *et. al.*, Phys. Rev. Lett. **70** (1993) 2515.
- [3] S. Berridge, *et. al.*, IEEE Nuc. Sci. **39** (1992) 1242.

ACKNOWLEDGEMENTS

I am especially grateful to my advisor, Raymond Frey, for his guidance and invaluable advice. I also owe a tremendous debt of gratitude to James Brau who encouraged and supported my graduate studies over many years.

I also thank the members of the University of Oregon Luminosity Group: Jennifer Huber, Matthew Langston, Kevin Pitts, Cary Zeitlin and Jingchen Zhou, as well as the members of the University of Tennessee Luminosity Group: William Bugg, Robert Kroeger, Achim Weidemann and Sharon White.

Many thanks to the Electroweak Group and all the members of the SLD Collaboration.

My appreciation also goes to the following people for their help, encouragement and friendship: Ram Ben-David, Philip Burrows, Richard Dubois, Robert Elia, Saul González, Sarah Hedges, Andrea Higashi, Amitabh Lath, Peter Rowson and John Yamartino

This work was only made possible with the support and love of my family and parents. I especially want to thank my wife, Hyunju Ku, for her support and patience.

TABLE OF CONTENTS

Chapter	Page
I. LEFT-RIGHT CROSS SECTION ASYMMETRY	1
Introduction	1
Theory	6
Summary of Physics Motivation	17
II. EXPERIMENTAL APPARATUS	18
Polarization at SLC	18
Polarimetry	28
Energy Spectrometer	39
Polarization Data Acquisition	40
Overview of the SLD	40
The Trigger and Data Acquisition	59
III EVENT SELECTION	61
Introduction	61
Event Selection Procedure	64
Background Estimation	87
Combined Efficiency of Triggering and Event Selection	92
IV POLARIZATION MEASUREMENT	96
Introduction	96
Measurement of the Compton Laser Polarization	98
Measurement of the Electron Beam Polarization	102
V ANALYSIS AND RESULT	114
Introduction	114
The A_{LR} Measurement	116
Corrections to A_{LR}	117
Total Systematic Error	122
Extraction of the Electroweak Mixing Parameter	122
Summary of Results	124
VI. DISCUSSION	130
Introduction	130
1993 A_{LR} Event Selection	130
Modification of 1992 Event Selection	136
Tracking Assisted Event Selection	145
REFERENCES	151

LIST OF TABLES

Table	Page
1.1 The Properties of the Gauge Bosons in the Standard Model	2
1.2 The Electroweak Properties of Fermions	5
3.1 Statistics Summary of Cuts for the Four Sample Runs: (1) is the Number of the LAC Tower Hits Cut, (2) is the Sum of the Total Tower Hit Energies Cut, (3) is the Sum of the Endcap WIC Pads Tower Energies Cut Along with the Total LAC Energy of Non-Isolated Tower Hits, (4) is the Energy Imbalance Cut, (5) is the Sphericity Cut Along with the Energy Imbalance Cut	77
3.2 Statistics Summary of the Three Filters for the 1992 Polarized Run: Numbers in the Second Column are the Number of Events which Passed the Filter at Each Stage	85
3.3 Double-Scanning Results	89
3.4 Results of the Maximum-Likelihood Method	90
3.5 Run Blocks for Hadronic Z^0 and Small-Angle Bhabha Events	93
3.6 Numerical Values Used for the Combined Efficiency	94
4.1 The Lead-in Calculated Analyzing Powers and the Average Measured Raw Asymmetries	110
4.2 Systematic Uncertainties from Polarization Measurement	111
5.1 Total Systematic Uncertainties in the A_{LR} Measurement	122
5.2 Corrections to the A_{LR} Measurement from Secondary Sources	125
6.1 Scan Results of Two Scanners	135

LIST OF FIGURES

Figure	Page
1.1 The Feynman Diagrams of Photon and Z^0 Exchange in $e^+e^- \rightarrow f\bar{f}$ at Tree-Level	7
1.2 The Cross Section of $e^+e^- \rightarrow f\bar{f}$ versus the Center-of-Mass Energy for 22% Longitudinally Polarized Electron Beam with 150 GeV Top Quark Mass and 100 GeV Higgs Mass: the Solid Curve is the Cross Section for Unpolarized Beam, the Dotted Curve is the Cross Section for -22% and the Dashed Curve is the Cross Section for +22% Polarized Electron Beam	9
1.3 The Feynman Diagrams of Photon and Z^0 Exchange in $e^+e^- \rightarrow e^+e^-$ at Tree-Level: (a) and (b) are the Contributions from s and t Channels, Respectively	10
1.4 The A_{LR} versus the Center-of-Mass Energy	11
1.5 Final State Gluon Radiation in $e^+e^- \rightarrow q\bar{q}$	12
1.6 The Electroweak Corrections such as the Oblique, Vertex, Box Corrections, and Bremsstrahlung Amplitudes: (a) involves γ and Z^0 , (b) and (c) involve γ , W^\pm , and Z^0 and (d) involves γ	13
1.7 A_{LR} versus the Top Quark Mass with Different Higgs Masses: the Solid Curve is for 100 GeV, the Dotted Curve is for 450 GeV, and the Dashed Curve is for 1000 GeV Higgs Mass	14
2.1 A Schematic Layout of the SLAC Polarized Linear Collider: the Direction of the Electron Spin Vector is Shown when the Electron Beam is Delivered from the Polarized Electron Source to the SLC Interaction Point	19
2.2 (A) is the Band Structure of GaAs. (b) Shows Energy Levels of the State: Solid and Dashed Arrows Show the Allowed Transitions after Absorbing Right- and Left-handed Circularly Polarized Photons, Respectively	22

2.3	A Negative Work Function is Accomplished by Deposition of a Cesium-Fluorine Monolayer on the Bulk GaAs Photocathode Surface: (a) is for Pure GaAs and (b) is for the GaAs with the Cesium Surface	22
2.4	The Polarized Light Source and Electron Source System	23
2.5	A Schematic Layout of the North Damping Ring: the Arrow Shown is the Electron Spin Direction	27
2.6	The Electron Beam Polarization Measurement with Compton Polarimeter as a Function of the Electron Beam Energy	29
2.7	The Betatron Effect on the Beam Polarization in the Arc due to the SLC Achromats	29
2.8	The Moller and Compton Polarimeters are Located at the End of the Linac and near the SLC Interaction Point, Respectively	30
2.9	A Schematic of the Moller Polarimeter	32
2.10	A Schematic of the Compton Light Source	34
2.11	A Schematic of the Compton Polarimeter	34
2.12	The Čerenkov Detector and the Proportional Tube Detector	36
2.13	The Compton Cross Section for Two Different Helicity Combinations of the Electron and Compton Laser Polarizations: the Degree of the Electron and Photon Polarization are Assumed to be 22.4% and 93%, Respectively	36
2.14	A Schematic of the Energy Spectrometer for Measurement of the Center-of-Mass Energy at the SLC	39
2.15	A Quarter of the Overall Layout of the SLD Detector	42
2.16	The Charged Coupled Device Vertex Detector in the Transverse Plane	43
2.17	The Luminosity Monitor System which Consisted of a Pair of the Luminosity Monitor and Small Angle Tagger (LMSAT) Detectors and the Medium Angle Silicon Calorimeters (MASC)	44
2.18	Well-Segmented Tower Geometry of the LMSAT for Providing Good Angular Resolution	44

2.19	The Layout of Wires in a Cell: the Field, Guard and Sense Wires are Represented by the Diagonal Crosses, Diamonds, and Circles, Respectively	46
2.20	Schematic of the Čerenkov Ring Imaging Detector Barrel Section which Shows Čerenkov Photons. There are Two Radiator Devices: One is a Liquid Radiator which is a Proximity Focusing Device and Other is a Gas Radiator which is a Ring Imaging Device with Gas	49
2.21	An Exploded View of the Barrel Section of the LAC	51
2.22	A Schematic of the Endcap Section of the LAC	52
2.23	A Logical Layout of the Barrel LAC Electronics	53
2.24	The Layout and Numbering of the Boards within the Barrel Tophat: The Solid Lines are for the Daughter Boards, Dotted Lines are for the Cryogenics Board and Dashed Lines are for the Controller and A/D Board	55
2.25	The Layout and Numbering of the Boards within the South Endcap Tophat: the Solid Lines are for the Daughter Boards, Dotted Lines are for the Cryogenics Board and Dashed Lines are for the Controller and A/D Board	55
2.26	A Diagram of the Tophat Signal Processing	56
2.27	A Schematic Diagram of the LAC Fastbus System	57
2.28	A Schematic of a Collection Point	58
3.1	Typical Hadronic Z^0 Event with LAC Tower Hits and Vectored Hits in the Central Drift Chamber	63
3.2	Typical Tau Pair Event	63
3.3	ADC Distributions of Tower Hits of Identified SLC Muons for Four LAC Layers: (a)-(d) are EM1, EM2, HAD1, and HAD2 Layers, Respectively	65
3.4	Typical SLC Muon Event which has Barrel LAC Tower Hits Parallel to the Beamline	68
3.5	The Distributions of N_{LAC} , E_{LAC} , E_{WIC}^{end} , E_{IMB} and SPHE of Monte Carlo Hadronic Z^0 Events	70

- 3.6 (A) is the Number of Tower Hits,
 (b) is the Total Energy of the LAC Tower Hits in the Four
 LAC Layers for All Triggered Events of the Four Sample Runs,
 (c) is the Total LAC Energy Distribution for the Events
 which Passed the N_{LAC} Cut 72
- 3.7 (A) is the Distribution of the Total LAC Energy and the Endcap WIC
 Energy for the Events which Passed the N_{LAC} Cut
 for the Four Sample Runs.
 (b) is the Same Distribution as (a) and,
 (c) is the Energy Imbalance Distribution for the Events
 which Passed the N_{LAC} and E_{TOT} Cuts,
 (d) is the Same Distribution as (c)
 except Applying One More Cut (3) 74
- 3.8 (A) is the Distribution of the Energy Imbalance and Sphericity for
 the Events which Passed Cuts (1), (2), and (3) for the Four
 Sample Runs,
 (b) is the Same Distribution of (a) after Cuts
 (1), (2), (3), and (4), and
 (c) is the Total LAC Energy Distribution
 of Non-Isolated Tower Hits after All Cuts Applied 75
- 3.9 The Distribution of N_{LAC} , E_{LAC} , E_{WIC}^{end} ,
 E_{IMB} , and SPHE of Events which Passed the First Filter
 for the All Triggered Events of the 1992 Polarized Runs 76
- 3.10 The Distribution of Total LAC Energy versus the Energy
 Imbalance for the Events which Passed the First Filter 78
- 3.11 The Distribution of the Sum of Four Maximum Electromagnetic Tower
 Energies versus Theta (binned in electromagnetic towers) for
 the Events which Passed the First Filter 78
- 3.12 Typical Wide-Angle Bhabha Event in the
 Endcap Liquid Argon Calorimeter 80
- 3.13 Suspicious Event (Presumably a Wide-Angle Bhabha) which has
 Lots of Energy Leakage in the Hadronic
 Layers at $T_{MAX} > 44$ 80
- 3.14 (A) is the Distribution of the Total LAC Energy
 and the Energy Imbalance,
 (b) is the Total LAC Energy Distribution, and
 (c) and (d) are the Total Energy Distributions in
 Regions (I) and (II), Respectively, for the
 Events which are Identified as Wide-Angle Bhabha 81

3.15 (A) is the Distribution of the Total LAC Energy and the Energy Imbalance, (b) is the Distribution of the Minimum Energy out of two Maximum Electromagnetic Tower Energies and the Energy Imbalance, (c) is the Distribution of the Total LAC Energy and the Minimum Tower Energy out of Two Maximum Electromagnetic Tower Energies for the Events which Passed the First Filter and were not Identified as Wide-Angle Bhabha	83
3.16 (A) is the Distribution of the E_{TOT} and the E_{IMB} after Cut (3), (b) is the Distribution of the $MIN(M1, M2)$ and the E_{IMB} after Cut (1), (c) is the Distribution of the E_{TOT} and the $MIN(M1, M2)$ after Cut (2), for the Events which Passed the First Filter and were not Identified as Wide-Angle Bhabha	84
3.17 (A) is the Distribution of the Total LAC Energy and the Θ_{bin} of the Tower having the Maximum EM1 Energy, (b) is Total LAC Energy Distribution, (c) is the Energy Imbalance Distribution, (d) is the Distribution of the Minimum Tower Energy out of Two Maximum Electromagnetic Tower Energies for the Final Selected Events	86
3.18 Total Number of Background Events in the Final Data Sample Based on the Maximum-Likelihood Method	90
3.19 Uncorrected Angular Distribution of the Final Sample Events	95
3.20 Efficiency Distribution of the LAC	95
4.1 A Schematic Diagram of the Compton Laser Polarization Monitor on the Compton Laser Bench	99
4.2 The Distribution of the Compton Laser Polarization on the Compton Laser Bench	99
4.3 A Schematic Diagram of the Pockels Cell Setup on the Compton Laser Bench	101
4.4 A Schematic Diagram of the Fresnel Prisms Setup on the Compton Laser Bench	101
4.5 The Dependence of the Unpolarized Compton Cross Section and Compton Asymmetry on the Distance (cm) from the Beamline in the Transverse Direction	103

4.6 Results of an Endpoint Scan for Channel 6: the Position Shown is the Detector Position from Nominal in cm Unit. Open Circles and Filled Circles are for EGS Simulation, and Data, Respectively	104
4.7 A_0 Measurement of the Polarimeter Runs for Monitoring the Time Dependence of the Position of the Zero-Asymmetry Point	105
4.8 Ratio of Signals of Detector Channel 7 to Channel 2 for Monitoring the Time Dependence of the Detector Calibration	106
4.9 The Measured Relative Asymmetry as a Function of the Phototube Pulse Heights for Channel 6	108
4.10 The Measured Relative Asymmetry as a Function of the Phototube Pulse Heights for Channel 7	108
4.11 The Measured Relative Asymmetry as a Function of the Phototube Pulse Heights for Channel 6 in the Well-Defined Unsaturated Region	109
4.12 The Measured Relative Asymmetry as a Function of the Phototube Pulse Heights for Channel 7 in the Well-Defined Unsaturated Region	109
4.13 Average Measured Compton Asymmetry over the Data Sample in the Detector for Seven Čerenkov Channels versus the Distance from the Beamline in the Transverse Direction (cm): the Compton Asymmetry Function is Fit to Data Using the Normalization Factor $\mathcal{P}_\gamma \mathcal{P}_e$	112
5.1 The Distribution of the Electron Beam Polarization of the Final Data Sample	115
5.2 The Time Dependence of the Electron Beam Polarization Measurement: The Solid Line Shown is the Luminosity Weighted Average Polarization Value	115
5.3 The Polarization Distribution (%) of the Left-Handed and Right-Handed Polarized Electron Beam	118
5.4 Beamstrahlung Asymmetry for Left- and Right-Handed Polarized Beam	121
5.5 Center-of-Mass Energy Distribution of the Final Data Set	123
5.6 Comparison of the Asymmetry Measurements with LEP Experiments	127

5.7	The Curve Gives the A_{LR} Dependence on the Top Quark Mass in the Minimal Standard Model for $M_H=200$ GeV: The 1992 A_{LR} Measurement is Given as Dotted and Dashed Bands for 68.3% and 95% Confidence Levels, Respectively. the Solid Band Gives the Errors Expected for the 1993 A_{LR} Measurement	128
5.8	T versus S_Z Plot for Γ_Z, Γ_{ee} and the 1992 A_{LR} Measurement: Each Circle and Cross Pair Represents the Standard Model Prediction for a Given Top Quark Mass, the Pair at Smallest T is for $M_T=100$ GeV, and the Next Pairs for $M_t=150, 200,$ and 250 GeV. The Circles and Crosses are for a Higgs Mass of 200 and 1000 GeV, Respectively	128
6.1	The Distribution of the Number of the Electromagnetic Tower Hits after Applying 60 ADC Counts Tower Threshold Cuts on the Electromagnetic Layers	131
6.2	Sum of Tower Hits Energy on the Four LAC Layers after Applying High (E_{HI}) and Low Tower (E_{LO}) Threshold Cuts on the Four LAC Layers	131
6.3	The Scatter Plot of the Total Energy Deposition of the Four LAC Layers versus the Energy Imbalance of the Events which Passed the Offline Hadron "Trigger"	134
6.4	(A): The Scatter Plot of the Number of Good Clusters for the LAC and the $ \cos\theta $ Value of the Thrust Axis, (b) and (c) are the Distributions of the Number of Good Clusters for $ \cos\theta < 0.8$ and $ \cos\theta \geq 0.8$, Respectively. The Lines are the Applied Number of Clusters Cuts Depending on $ \cos\theta $	134
6.5	The Distribution of the Total LAC Tower Hits Divided by the Total LAC Energy versus $ \cos\theta $ of the Thrust Axis	137
6.6	The Scatter Plot of the Energy-Weighted Hits (EWH) versus the Hit-Weighted Energies (HWE) for the 1992 A_{LR} Data Sample for $ \cos\theta < 0.95$	138
6.7	The Scatter Plot of the Energy-Weighted Hits (EWH) versus the Hit-Weighted Energies (HWE) for the Events which Passed the KZ0FLT Filter for $ \cos\theta < 0.95$	138
6.8	The Scatter Plot of the Energy-Weighted Hits (EWH) versus the Hit-Weighted Energies (HWE) for the 1992 A_{LR} Data Sample for $ \cos\theta \geq 0.95$	139